Journal of Applied Polymer Science

Selective Etching of Polylactic Acid in Poly(styrene)-block-Poly(D,L)lactide Diblock Copolymer for Nanoscale Patterning

Cian Cummins,[1] Parvaneh Mokarian-Tabari,[1,2] Justin D. Holmes,[1,2] Michael A. Morris[1,2]
[1]Materials Research Group, Department of Chemistry and Tyndall National Institute, University College Cork, Cork, Ireland
[2]Centre for Research on Adaptive Nanostructures and Nanodevices (CRANN), Trinity College Dublin, Dublin, Ireland
Correspondence to: P. Mokarian-Tabari (E-mail: p.mokarian@ucc.ie)

ABSTRACT: Self-assembled thin films of a lamellar forming polystyrene-*block*-poly(D,L)lactide (PS-*b*-PLA) block copolymer (BCP) contain a "reactive" block that can be readily removed to provide a template for substrate pattern formation. Various methods of PLA removal were studied here with a view to develop the system as an on-chip etch mask for substrate patterning. Solvo-microwave annealing was used to induce microphase separation in PS-*b*-PLA BCP with a periodicity of 34 nm (L_o) on silicon and silicon on insulator (SOI) substrates. Wet etches based on alkaline and enzymatic solutions were studied in depth. Fourier transform-infrared (FT-IR) analysis showed that basic hydrolysis using sodium hydroxide (NaOH) or ammonium hydroxide (NH_4OH) solutions resulted in greater PLA removal in comparison to an enzymatic approach using Proteinase K in a Tris-HCl buffer solution. However, in the enzymatic approach, the characteristic self-assembled fingerprint patterns were retained with less damage. Comparison to a dry etch procedure using a reactive ion etch (RIE) technique was made. A detailed study of the etch rate of PS and PLA homopolymer and PS-*b*-PLA shows depending on DC bias, the etch selectivity of PLA and PS $\left(\frac{dPLA}{dPS}\right)$ can be almost doubled from 1.7 at DC bias 145 V to 3 at DC bias 270 V. © 2014 Wiley Periodicals, Inc. J. Appl. Polym. Sci. **2014**, *131*, 40798.

KEYWORDS: biodegradable; self-assembly; copolymers; microscopy; nanostructured polymers

Received 10 February 2014; accepted 29 March 2014
DOI: 10.1002/app.40798

INTRODUCTION

Block copolymers (BCPs) consist of two chemically incompatible polymers covalently bonded that can microphase separate into well-arranged nanoscale features of significant nanotechnological importance.[1–5] By altering molecular weights and volume fractions of the BCP components, the periodicity of the resulting morphology can be controlled and the pattern can be developed for a particular function. In recent years, there has been much interest in BCPs for nanolithography use due to these tuneable characteristics.[6,7] With the ability to achieve sub-10 nm feature sizes[8,9] and integrated circuit relevant geometries through directed self-assembly,[10–12] BCPs are a possible alternative methodology for further extension of Moore's Law.

One of the key processes in a strategy for developing high density device structures from BCPs is pattern transfer where the "soft" mask is transferred to the underlying substrate. It is highly desirable to have a BCP system where one block can be readily removed (etched) to form a topographic pattern resistant block acting as an on-chip mask for subsequent substrate etching. This process is well demonstrated for the polystyrene-*block*-polymethylmethacrylate (PS-*b*-PMMA) system using reactive ion etching (RIE).[13–17] Controlled wet etching can also be effective and because of its simplicity may be practical as a general method to create periodic porous nanochannels[18] for inclusion of functional material for applications in optical, medical or sensing technologies.

The development of processes for selective block removal and/or subsequent pattern transfer is challenging and several solutions have been trialled. An "*in situ*" inclusion technique recently showed the effectiveness of metal oxide etch masks as size and dimensional control were demonstrated for silicon nanopillar and nanowire fabrication.[19–21] Polystyrene-*block*-polydimethysiloxane (PS-*b*-PDMS) has also been intensely studied as the silicon backbone of the PDMS block provides natural etch contrast and can form a robust template for pattern transfer purposes.[8] Polystyrene-*block*-polylactide (PS-*b*-PLA) is another BCP of considerable potential as an etch mask or porous forming template. Firstly, PS-*b*-PLA has a high Flory Huggins interaction parameter ($\chi = 0.233$)[22] which makes smaller feature sizes more accessible. Secondly, PS-*b*-

Additional Supporting Information may be found in the online version of this article.

© 2014 Wiley Periodicals, Inc.

PLA has similar block surface energies avoiding wetting layer formation at the polymer/air interface. Lastly, the ease of removal of the aliphatic polyester PLA makes the system ideal for attaining high etch contrast. PLA has been etched most commonly using a mild NaOH solution.[23–26] It has also been suggested that a PLA wetting layer exists at the polymer/substrate interface and this can cause delamination without suitable surface treatment.[27,28] This approach of substrate modification was recently used for a bottlebrush PS-*b*-PLA where an enzyme was used for PLA degradation to replicate biological conditions.[29]

This work demonstrates the applicability of PS-*b*-PLA in pattern transfer through the use of a highly selective dry etch procedure to remove the PLA block and enable silicon nanowire fabrication. Three wet etch routes to remove PLA were also studied. The often used NaOH was shown to result in over etching. This led to development of an NH_4OH and methanol etch system. We also report extension of established enzymatic PLA degradation in biomedical studies[30–34] to degradation of the PLA block in PS-*b*-PLA system. As mentioned, the dry etching of PLA could be performed with a high degree of selectivity leading to large area removal of PLA with the structure of the original pattern being retained. The etch selectivity of PS and PLA was measured in a controlled way by manipulating the DC bias indirectly during the RIE process.

EXPERIMENTAL

Materials

Planar substrates used were highly polished single-crystal silicon <100> wafers (*p*-type) with a native oxide layer of ~2 nm. No attempt was taken to remove the native oxide of a few nanometers depth. Silicon on insulator (SOI) substrates employed contained a 140 nm box layer on bulk silicon, followed by a gate oxide with a thickness of 1.2 nm, a 50 nm device active layer, and finally a 20 nm silicon dioxide layer. Polystyrene-*block*-polylactide (referred to as PS-*b*-PLA, note that PLA is in the DL form) was purchased from Polymer Source, Inc., Canada, with a total number average molecular weight of $M_n = 40.5$ kg mol^{-1} ($M_{nPS} = 21$ kg mol^{-1}; $M_{nPLA} = 19.5$ kg mol^{-1}, $f_{PS} = 0.53$), a polydispersity index of 1.15 and was used as received. Hydroxyl terminated polystyrene (PS-OH) was purchased from Polymer Source, Inc., Canada, with a total number average molecular weight of $M_n = 6$ kg mol^{-1}, a polydispersity index of 1.05 and was used as received. PS and PLA hompolymer ($M_{nPS} = 16$ kg mol^{-1} with a polydispersity index of 1.03 and $M_{nPLA} = 16$ kg mol^{-1} with a polydispersity index of 1.30) were both purchased from Polymer Source, Inc., Canada. Proteinase K (from Tritirachium album lyophilized powder), sodium hydroxide beads, ruthenium (III) chloride hydrate, ammonium hydroxide (28.0–30.0% NH_3 basis), methanol (anhydrous, 99.8%), chloroform (HPLC grade, ≥99.9%, contains 0.5–1.0% ethanol as stabilizer), tetrahydrofuran (THF) (HPLC grade, ≥99.9%) and sodium hypochlorite solution (reagent grade, chlorine 10–15%) were all purchased from Sigma Aldrich. Ruthenium tetroxide (RuO_4) was prepared as described elsewhere[35] and staining was carried out for 1 min.

Substrate Cleaning, PS-OH Brush Modification, BCP Preparation, Homopolymer Preparation, and Deposition

Substrates were cut into pieces that allowed for horizontal placement in microwave tube. Initial experiments involved cleaning substrates using UV/ozone for 30 mins before solvo-microwave annealing. All UV/Ozone treatments were performed in a PSD Pro Series Digital UV Ozone System, Novascan Technologies, Inc. However, when BCP films prepared on UV/ozone cleaned substrates were wet etched delamination of the film resulted. Thus, substrates were modified with a PS-OH brush to promote more stable films. Further examination on substrate surface modification is discussed below. For PS-OH brush modified surfaces, substrates (Si or SOI) were degreased by ultrasonication in acetone and isopropanol (IPA) solutions for 5 mins each, dried in flowing nitrogen gas and baked for 2 mins at 180°C in an ambient atmosphere to remove any residual IPA. This was followed by cleaning in a piranha solution (*1:3* v/v 30% H_2O_2:H_2SO_4) (*Safety caution: May cause explosion in contact with organic material!*) at 100°C for 60 mins, rinsed with deionized water (resistivity ≥ 18 MΩ/cm) several times and dried under nitrogen flow; 1 wt % PS-OH solutions in toluene were then spin coated at 2000 rpm for 30 sec. After spin coating, substrates were annealed at 180°C for 6 h. PS-OH treated substrates were rinsed in toluene for 10 mins twice to remove any excess polymer that had not grafted fully to the substrate surface. After washing, substrates were blown dry with nitrogen gas. An ellipsometry measurement shows a 2 nm brush layer is formed; 2 wt % PS-*b*-PLA solutions were made using chloroform whereby the solution was sonicated for 30 mins to ensure full dissolution. Following dissolution, BCP solution was spin coated on the PS-OH brush modified surfaces at 2000 rpm for 30 sec. For hompolymer dry etch studies only, 3 wt % chloroform solutions of PS and PLA films were prepared and spin coated at 2000 rpm on UV/ozone cleaned silicon substrates.

Microwave Annealing Process

Please note that a comprehensive study will be published in due course on the solvo-microwave annealing of this PS-*b*-PLA system. Following deposition of the BCP solution at 2000 rpm for 30 sec, patterns were developed after samples were placed in the sample holder (i.e. microwave tube) and then placed in the microwave (CEM model). Note that the experimental setup including the microwave holder and the microwave synthesizer can be viewed elsewhere.[6] Power was set at 300 W, while ramp rate was set for 3 mins, and temperature was set to 55°C with THF as solvent in the sample holder. Annealing time varied from 15 sec to 2 mins.

PLA Etching Methods

Alkaline Route 1. A 0.05*M* NaOH (60 : 40, water : methanol) solution was prepared at room temperature. The solution was given sufficient time (~15 mins) in order to fully dissolve. Microwave annealed PS-*b*-PLA films were then immersed in the solution for a range of time periods. After removal, films were washed twice with deionized water/methanol for 5 mins.

Alkaline Route 2. NH_4OH/methanol (1:2) solution was prepared at room temperature. The same procedure as NaOH approach was followed for immersion and washing of the film.

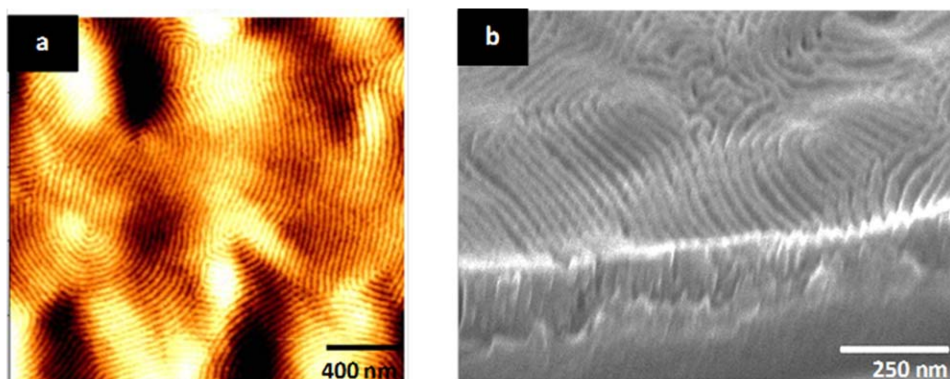

Figure 1. (a) AFM topography image of microphase separated PS-*b*-PLA structure on UV/ozone cleaned silicon substrate after solvo-microwave annealing for 60 sec in the presence of THF at 55°C. Film thickness was measured at ~200 nm. (b) Cross-section SEM image of the initially microphase separated structure on silicon following staining with RuO_4. [Color figure can be viewed in the online issue, which is available at wileyonlinelibrary.com.]

Enzymatic Route. The degradation solution here composed of 1 mg of Proteinase K dissolved in 5 mL of Tris-HCl buffer (pH = 8.6). The solution was placed in an oil bath and left heat to 37°C. Once the desired temperature was reached, and stable for a period of time, the PS-*b*-PLA films were immersed for various times (from 15 mins to 24 h). Following degradation, the film was removed and washed twice in deionized water for 5 mins. All films were washed as described above and were dried under nitrogen flow to ensure complete removal of PLA fragments that were degraded.

Dry Etch Tools and Recipes

Dry etching of the PS-*b*-PLA films was performed in an Oxford Instruments Plasmatech in RIE mode using a mixture of argon and oxygen gas. Flows rates were set at 15 sccm for argon and 10 sccm for oxygen gas. Process pressure was 12 mTorr while radio frequency power was 40 W. The value of DC bias was varied between 145V and 270V which is a critical parameter by altering process pressure. The DC bias variation proved to be a critical parameter for result consistency. This is discussed in detail in the Result and Discussion section.

Pattern Transfer. The remaining PS etch mask was pattern transferred to the underlying silicon substrate using a combination of sulphur hexafluoride (SF6) and trifluoromethane (CHF3) gasses in an STS AOE inductively coupled plasma (ICP) etcher.[17] The residual PS stripes following the pattern transfer were removed by O_2 plasma.

Characterization

Film Thickness. BCP film thicknesses were measured with a spectroscopic ellipsometer "J.A. Woollam Ellipsometer" at a fixed angle of incidence of 70°, on at least five different places on the sample and was averaged as the film thickness. A three layer model (SiO_2 + polymer brush + BCP) for total BCP film was used to simulate experimental data.

Atomic Force Microscopy (AFM). AFM (Park systems, XE-100) was operated in AC (tapping) mode under ambient conditions using silicon microcantilever probe tips with a force constant of 42 N m^{-1}. Topographic and phase images were recorded simultaneously. AFM was employed to monitor the progression of each etch route and since AFM cannot define the exact depth etched in the PS-*b*-PLA samples, etch values quoted here are nominal. However, the relative magnitude of the etch depth observed agreed with cross-section SEM measurements and so could be used for comparative purposes.

Scanning Electron Microscopy (SEM). SEM images were obtained by a FEI Helios Nanolab 600i system at an accelerating voltage of 5 kV and at a working distance of 4 mm. Cross-section SEM images involved cleaving the substrate in half and positioning the substrate perpendicular to the incident beam of electrons. The stage was then tilted at 20°.

Fourier Transform-Infrared (FT-IR) Spectroscopy. An IR660, Varian infrared spectrometer was used to record the FT-IR spectra. The FT-IR was operated in ATR mode. The measurements were performed in the spectral range of 4000 to 400 cm^{-1}, with a resolution of 4 cm^{-1} and data averaged over 32 scans. This characterization was carried out to see the effect of the etch routes on degradation of the PLA composition.

RESULTS AND DISCUSSION

Self-Assembly and Surface Modification

Microwave annealing is an emerging technique for inducing microphase separation in BCPs in a quick, easy and low cost manner. Zhang et al.[36] published the seminal work illustrating its flexibility for the rapid self-assembly of PS-*b*-PMMA and PS-*b*-P2VP (polystyrene-*block*-poly2vinylpyridine) BCPs. Borah et al. recently demonstrated microwave annealing without the use of solvents for self-assembly of PS-*b*-PMMA[37] and PS-*b*-PDMS[8,37] block copolymer systems. Here solvo-microwave annealing was used to generate highly ordered lamellar PS-*b*-PLA patterns (see experimental for details). A fingerprint pattern with a periodicity of 34 nm (L_o) was formed [see Figure 1(a)]. The solvo-microwave annealed films had a thickness of 200 nm following self-assembly. The initial self-assembled pattern in Figure 1(a) is the PS-*b*-PLA film without any etching and is characteristic of films used for wet and dry etching procedures below. Due to the similar surface energies of PS and PLA ($\gamma_{s\ PS}$ = 42.0 mJ m^{-2}, $\gamma_{s\ PLA}$ = 36.0–41.1 mJ m^{-2}),[27] a preference for either block at the polymer/air interface does not exist and since a neutral solvent THF (solubility parameters for PS, PLA and THF are 18.5 $MPa^{1/2}$, 18.5 $MPa^{1/2}$, and 16.8 $MPa^{1/2}$, respectively)[38] was used for annealing,

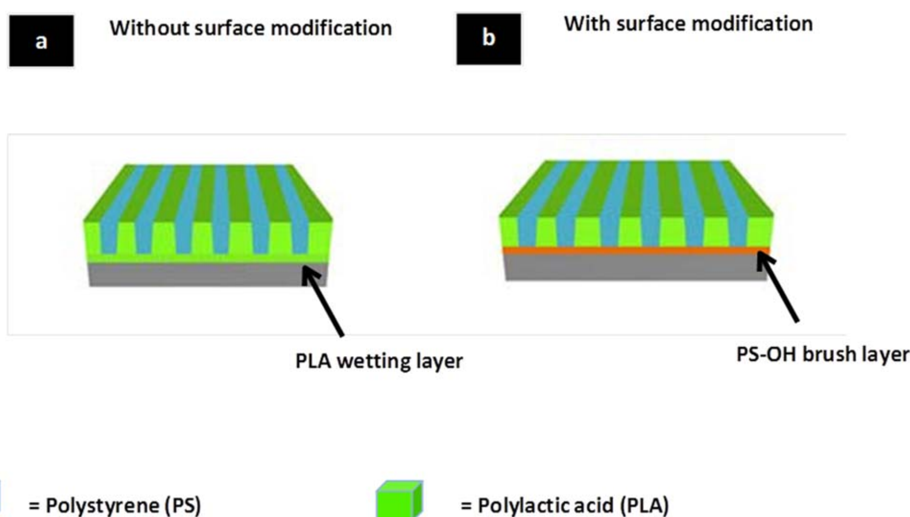

Scheme 1. Graphical representation of interfacial interaction of PS-*b*-PLA with different substrate chemistries, (a) after UV/O_3 treatment only and (b) after piranha cleaning plus grafting of PS-OH brush. [Color figure can be viewed in the online issue, which is available at wileyonlinelibrary.com.]

perpendicular lamellar patterns were observed. THF was introduced to enable self-assembly as the polymer chains are mobilized by the solvent vapor during the rapid annealing process. Microwave annealing was carried out without solvent but did not produce microphase separated patterns. Dewetting is not an issue like other high χ BCP materials such as PS-*b*-PDMS where the large surface energy difference between the blocks results in preferential wetting at polymer/substrate and polymer/air interfaces.[39,40] The PS-*b*-PLA film shows complete surface coverage (see Supporting Information Figure S1). For SEM characterization of

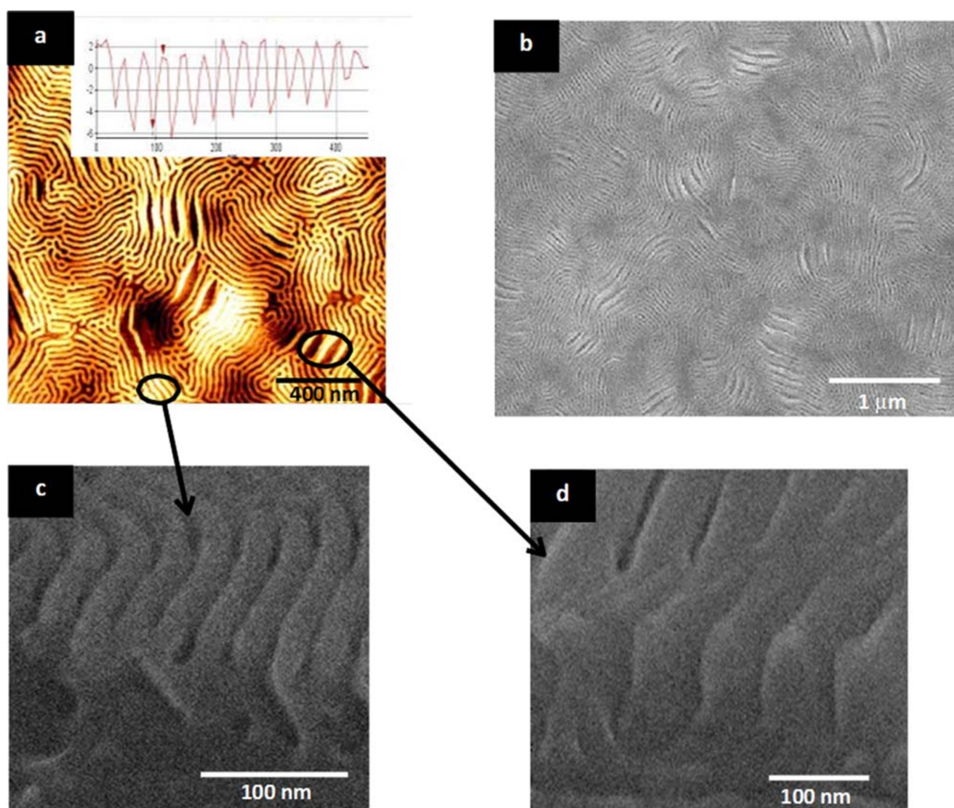

Figure 2. (a) AFM topographic image (2 × 2 μm) after 5 mins etching with 0.05*M* sodium hydroxide/methanol solution. Inset shows AFM line profile estimating PLA degradation of 6.5 nm. (b) Low-resolution top down SEM image of (a). (c) Cross-section SEM image showing an area that has retained the periodicity (34 nm) of the original pattern. (d) Cross-section SEM image of a region where PS lines have coalesced. [Color figure can be viewed in the online issue, which is available at wileyonlinelibrary.com.]

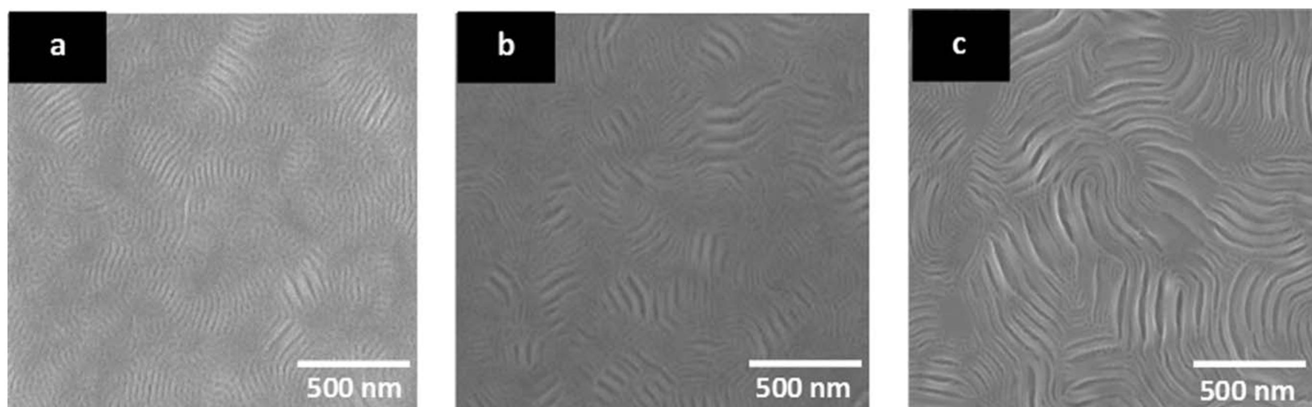

Figure 3. Top down SEM images of partial PLA degradation using 0.05*M* sodium hydroxide/methanol solution. (a) 15 mins immersion, (b) 30 mins immersion, (c) 45 mins immersion.

the microphase separated structure, staining with RuO_4 was used to enhance the domain contrast between PS and PLA. Figure 1(b) shows a cross-section SEM image of the self-assembled PS-*b*-PLA pattern where PS domains appear bright in comparison to the dark PLA domains. The image provides evidence for the extension of the lamellar through the entire film.

It should be noted that initial experiments involving exposure of the films to NaOH solutions of varying concentration resulted in immediate delamination of the BCP thin film after immersion. We believe this is due to the formation of a PLA wetting layer at the polymer-substrate interface as shown in Scheme 1(a). This wetting mechanism has been postulated in previous work[27] and is probably due to strong polar interactions of PLA with the native silicon oxide layer. Thus, degradation of the PLA wetting layer in NaOH leads to detachment of the polymer film and delamination. To avoid this problem, a PS-OH brush layer was grafted to piranha cleaned Si or SOI substrates using thermal annealing enabling better adhesion of the polymer film through the increased PS block interaction with the treated surface. Polymer brushes are commonly used to control microdomain orientation[8,37] but the functionalization used here did not modify the pattern formation significantly and was successful in promoting effective selective etching even in harsh conditions. We believe the brush aids layer homogeneity and thus the increased PS block interaction with the modified substrate allows wet etching to be carried without film delamination. As mentioned, the existence of a PLA wetting layer is speculated due to the dramatic loss of film during wet etching. We are unable to determine the existence of a thick BCP wetting layer (i.e. PS wetting layer) when the PS-OH brush is used for surface functionalization. Since we speculate the absence of a thick PS wetting layer, our illustration in Scheme 1(b) shows a PS-OH brush modification layer enabling PS-*b*-PLA self-assembly comparable to non-treated substrates, i.e. domains are ordered perpendicular to substrate.

PLA Degradation with Sodium Hydroxide Route

Hillmyer et al. have shown that basic hydrolysis is suitable for the removal of the PLA block in asymmetric PS-*b*-PLA systems.[23–25,27,28,38,41] Figure 2 displays AFM and SEM data following the etching of a PS-*b*-PLA film with 0.05 M NaOH for 5 mins. The solution degraded 6.5 nm on average of PLA from the AFM line profile. Figure 3 shows SEM data of etching PS-*b*-PLA films with 0.05 M NaOH for 15, 30 and 45 mins respectively (see corresponding AFM data in Supporting Information

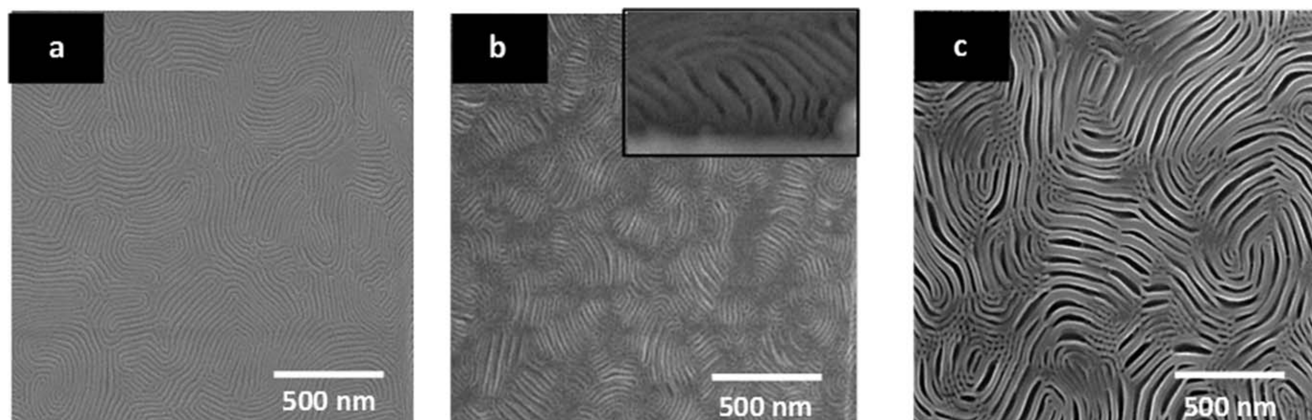

Figure 4. Top down SEM images of partial PLA degradation using an ammonium hydroxide/methanol solution. (a) 10 mins immersion, (b) 20 mins immersion, (c) 30 mins immersion. Inset in (b) shows cross-section of film.

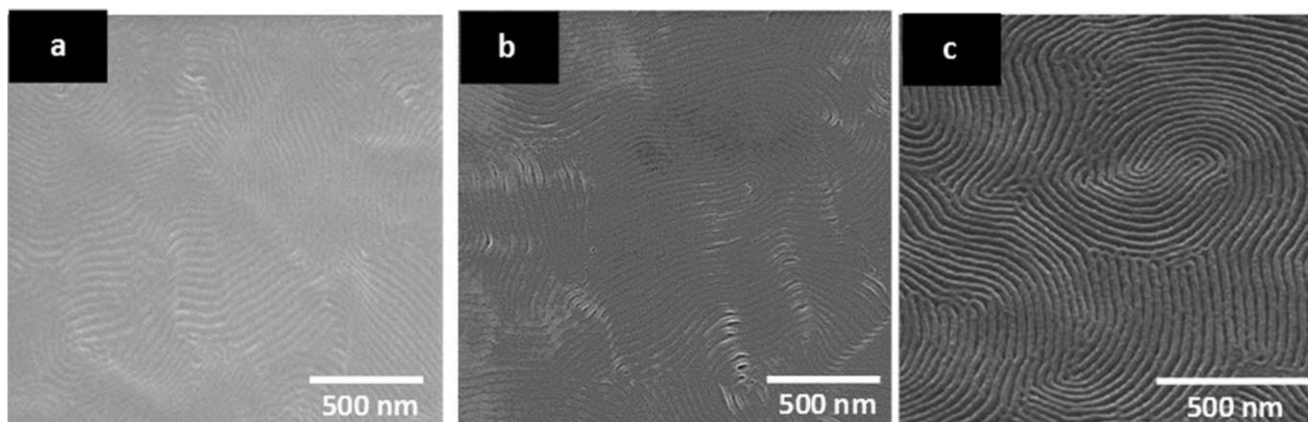

Figure 5. Top down SEM images of PS-*b*-PLA samples after immersion in a Proteinase K/Tris-HCl buffer (pH = 8.6) solution at 37°C for (a) 15 mins, (b) 30 mins, (c) 45 mins. Note SEM image (c) is at a tilt of 45°.

Figure S2); 10 nm of PLA was etched on average with 15 mins treatment (see Supporting Information Figure S3). Etching the films for 30 and 45 mins resulted in degradation and damage to the film pattern. This suggests that a 5 to 15 min treatment period is the optimum process window for the NaOH etch solution for degrading PLA.

The concentration of the NaOH solution (0.05*M*) is 10 times less than previously reported for hexagonal forming PS-*b*-PLA systems,[23,38,41] yet considerable structure deformation was observed. Using a 0.5*M* NaOH solution and exposure times of 5 mins led to complete removal of the pattern formed and this suggests that lamellar patterns are more susceptible to pattern destruction during selective removal of PLA. This could be due to a number of factors. The hexagonal phase may have greater structural integrity due to the honeycomb like structure of PS that remains after removal. The crystallinity of PLA is an important factor that can define the etch degradation rate. PLA etched in some previous studies[42,43] were of a highly crystalline PLLA form compared to the amorphous PLA in our system. The PLA here is in the DL isomeric or racemic form. The crystalline form is probably less soluble due to the crystalline stabilization energy[44] and amorphous regions allow water uptake more readily.[45] Finally, because the films here are relatively thick, the PS fin-like structures may have little mechanical robustness and collapse into one another. This merging of features can be seen in Figures 2, 3(a–c), and 4(b,c). Specifically, Figure 2(c) illustrates the success of PLA removal whilst retaining the microphase separated periodicity of 34 nm. In contrast, some areas as shown in Figure 2(d) reveal merging of the PS fin-like structures with a periodicity of 70 nm.

PLA Degradation with Ammonium Hydroxide Route

Because of the sensitivity of the system to caustic solutions, an alternative alkaline solution was sought. In basic aqueous solutions like NaOH solutions described above, PLA is vulnerable to main chain cleavage leading to the degradation of PLA and water uptake.[46] Subsequently, hydrolysis of —C—O— ester bonds occurs.[47] Thus, a solution of ammonium hydroxide and methanol to reduce the rate of hydrolysis was investigated.

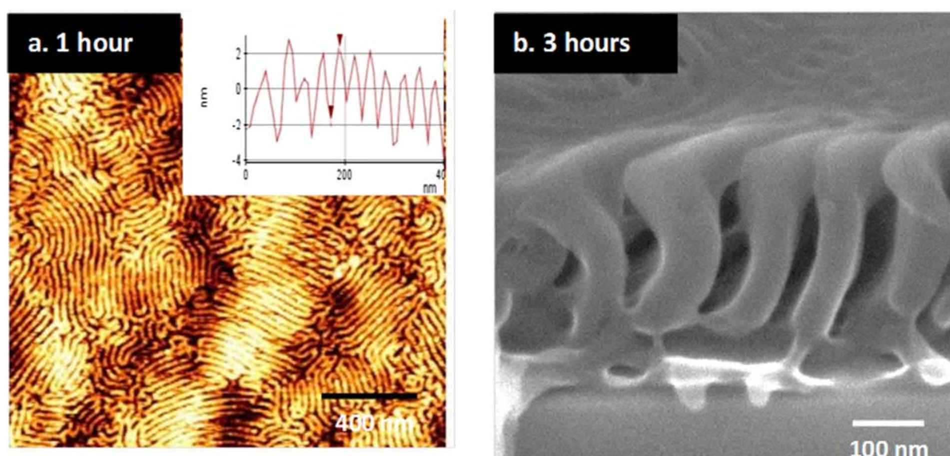

Figure 6. (a) AFM topographic image (2 × 2 μm) after 60 mins etching with Proteinase K/Tris-HCl buffer (pH = 8.6) solution at 37°C. Inset shows estimated 5 nm etched from AFM line profile. (b) Cross-section SEM image after immersing in Proteinase K Tris-HCl buffer solution for 3 h. [Color figure can be viewed in the online issue, which is available at wileyonlinelibrary.com.]

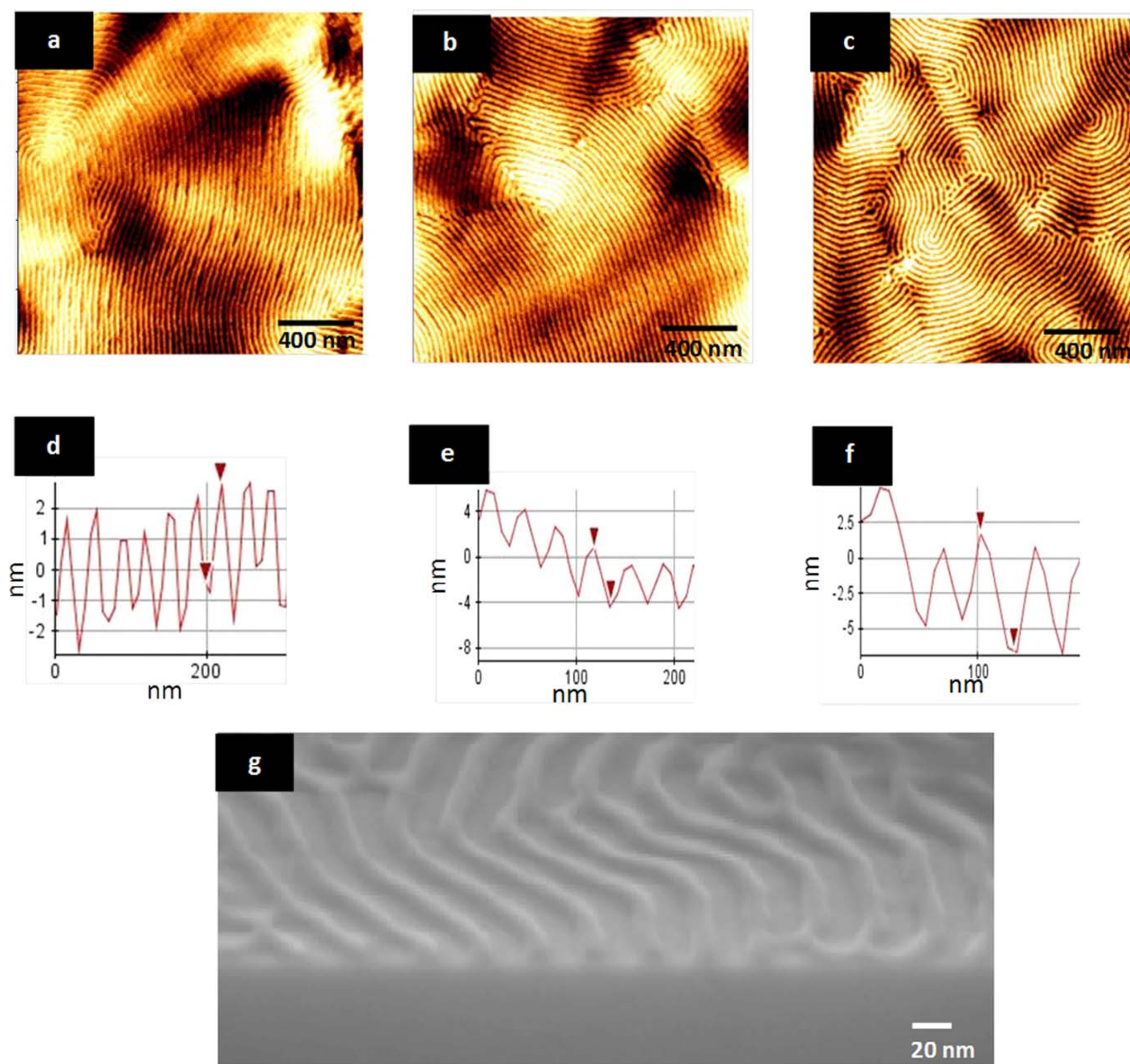

Figure 7. AFM topographic images (2 × 2 μm) after the selective removal of PLA using a reactive ion etching combination of argon and oxygen gas. Dry etching was carried out for (a) 10 sec, (b) 15 sec, and (c) 20 sec. (d) and (f) are AFM line profiles of etch depth of (a–c). (g) Cross-section SEM image of PS-*b*-PLA film after 20 sec RIE. [Color figure can be viewed in the online issue, which is available at wileyonlinelibrary.com.]

Figure 4 shows top down SEM images of this approach using etch times of 10, 20 and 30 mins respectively (see Supporting Information Figure S4 for corresponding AFM data). Excellent etch contrast is observed similar to the PS-*b*-PLA films treated with the NaOH solutions. However, isolated regions of pattern collapse are first observed after 20 mins of etchant exposure as shown in Figure 4(b) (note that the inset in b shows varying periodicity of the PS fin-like structures as seen above for the NaOH route). The amount of PLA removed after 30 mins etching with NH_4OH solution was estimated to be 15 nm from AFM line profile (see Supporting Information Figure S5) suggesting significant PLA removal. The top down SEM image in Figure 4(c) confirms coalescence of PS lines and the apparent domain size has increased considerably. A contributing factor to this coalescence is the high aspect ratio of the polymer films. Since the films are quite thick (~200 nm), they are not mechanically robust enough, and thus with the increased aspect ratio following PLA removal the PS lines will collapse into one another. This has also been previously demonstrated for thick PS-*b*-PMMA films during wet etching.[48]

The loss of the pattern quality on extended etching could be attributed to autocatalysis (i.e. product catalysed reaction[49]). Autocatalysis in PLA is caused by initial hydrolysis yielding carboxylic acid terminated chains that subsequently catalyse ester hydrolysis. For PDLLA, autocatalysis occurs faster within a

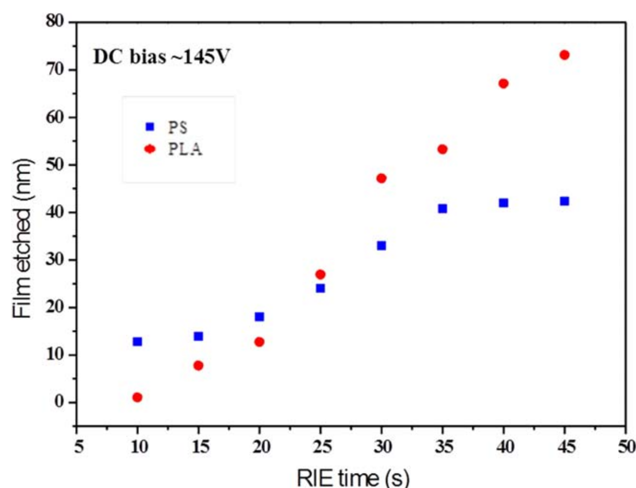

Figure 8. The etch rate of PS and PLA homopolymers in RIE at DC bias 145 V. Initially PLA shows slower etch rate due to high sputtering yield C=O group, but after 20 sec when the C=O bond is broken, PLA is etched faster than PS. [Color figure can be viewed in the online issue, which is available at wileyonlinelibrary.com.]

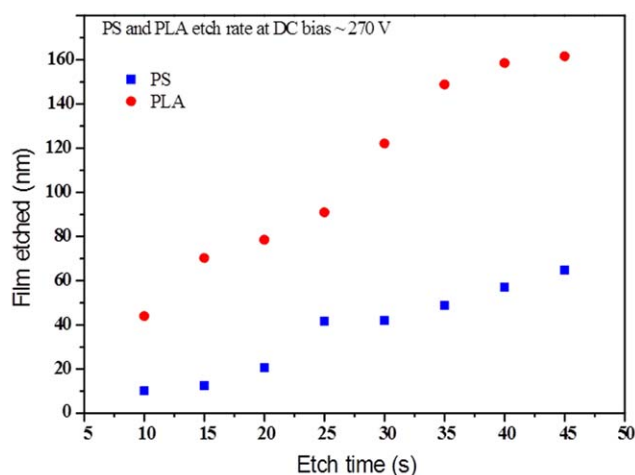

Figure 10. PS and PLA homopolymer etch rate at DC bias ~270 V. [Color figure can be viewed in the online issue, which is available at wileyonlinelibrary.com.]

PDLLA structure than at the surface[47] and this might account for the delamination observed in the non-brush coated substrates as well merging of the PS features rather than simple thinning of the structures. Note that little surface etching is observed. An AFM line profile obtained prior to etching shows the PS domains have a width of 23 nm for self-assembled patterns. However, after a sample was exposed to the NH_4OH etch for 30 mins, the domain width doubled to 46 nm, a periodicity consistent with merging of two adjacent PS lines as described earlier.

PLA Degradation with Enzymatic Route

Whilst both alkaline solutions showed promise as PLA etchants, they both showed extensive pattern damage at extended periods prior to complete PLA removal. For successful use in pattern transfer both complete removal and low damage are

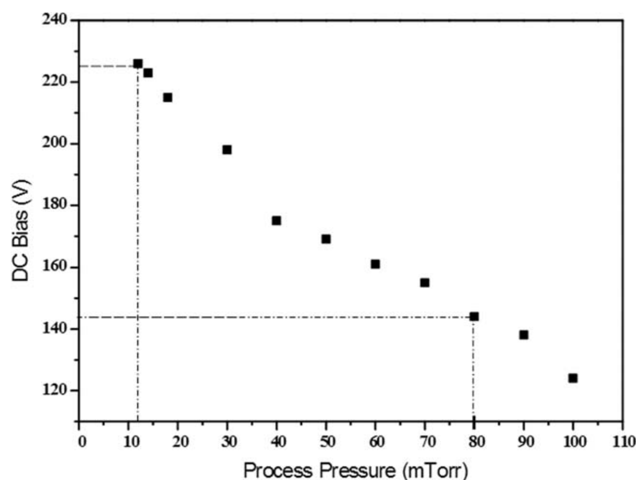

Figure 9. Calibration of DC bias via process pressure. Increasing the process pressure reduces DC bias. A Good control and monitoring the DC bias is critical for stability and consistency of the results in RIE etch process.

pre-requisites so that low line edge roughness and good aspect ratio are achieved. Thus, an alternative methodology of biodegradation was examined. PLA is a polymer that can be degraded through the action and metabolism of microorganisms yielding non-toxic products.[50] Although we have described this method here as enzymatic, it should be noted that degradation using Proteinase K combines both enzymatic and chemical hydrolysis.[51] This enzymatic approach is novel since PLA biodegradation is common in food science and biomedicine but has yet to be employed with diblock copolymers. Following documented conditions[26,52] to mimic a biological environment, we used Proteinase K enzyme in a Tris-HCl buffer solution (pH = 8.6) at 37°C. Top down SEM images following different exposure times to the enzymatic environment are shown in Figure 5 (see Supporting Information Figure S6 for corresponding AFM data). Although the rate of PLA removal is significantly less than for the basic hydrolysis etches, the SEM data are of high quality consistent with a highly homogeneous etch over the whole of the surface. Additionally, after 45 mins of etching the polymer film retained the characteristic fingerprint pattern with little sign of damage [Figure 5(c)]. FT-IR data confirms that at least 50% of PLA is removed in the bulk film.

Further enzymatic degradation studies were carried out at extended etch periods. Exposing the film for 1 h to the enzymatic conditions produced good porous templates with 5 nm of PLA removed over large areas as shown in Figure 6(a). Indeed, non-destructive removal of PLA with Proteinase K could be observed for up to 3 h when extensive damage can be seen as the PLA concentration became very low [see SEM images Supporting Information Figure S8(a–e)]. The cross-section SEM of the sample etched in the Proteinase K solution for 3 h is shown in Figure 6(b) revealing the PS topography after PLA removal. As observed previously for extended etching with the alkaline solutions described above, merging of the PS structures is seen in isolated areas.

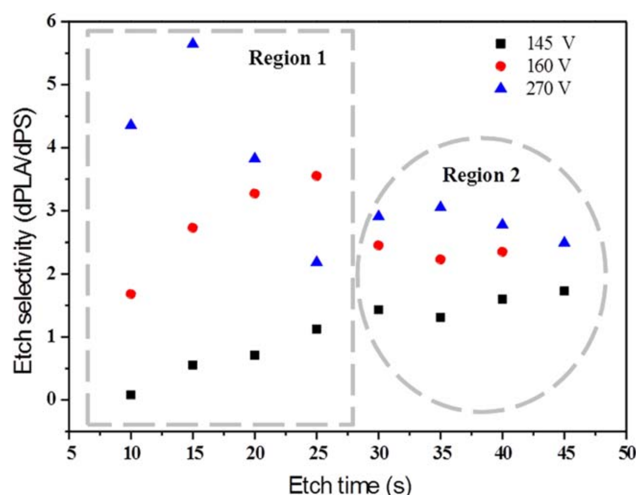

Figure 11. The effect of DC bias on etch selectivity of PS and PLA homopolymers. The fluctuation of DC bias at the beginning of RIE etch leads to unstable etch selectivity (region 1). The effect is more noticeable for higher values of DC bias (270 V in region 1). At longer times when the fluctuation is less, the etch selectivity remains mostly unchanged at any given DC bias (region 2). However, the etch selectivity is greater at higher DC bias values. [Color figure can be viewed in the online issue, which is available at wileyonlinelibrary.com.]

Dry Etch Studies and Route for PLA Removal

A dry etch process was also optimized to selectively remove an estimated 10 nm of PLA as determined from AFM line profiles. In Figure 7, AFM images a–c highlight the stepwise removal of PLA using a combination of argon and oxygen plasma with a reactive ion etcher (see Experimental for details). The AFM topographic images are of high quality and show little damage over large areas. Figure 7(d–f) shows the corresponding line profiles of AFM images (a–c). The resulting dry etch structures show a highly selective etch. PLA is etched at a faster rate than PS due to the presence of oxygen in PLA. It has been calculated from our experimental studies that the etch selectivity for PS-*b*-PLA is 1 : 5 (PS : PLA) which is significantly greater than that quoted for the PS-*b*-PMMA system (ranges from 1.5 to 2.5).[53] In comparison to the wet etch methodologies carried out here, the dry etch process is extremely quick, highly selective and nondestructive to the PS component. The cross-section SEM image in Figure 7(g) highlights this as a well-defined PS soft mask template has been created following RIE for 20 s.

Detailed etching experiments on homopolymers (PS and PLA) and diblock copolymer (PS-*b*-PLA) thin films were carried out to understand the removal rates and behavior of films following the dry etch procedures. The etch rate of polymers has been demonstrated to be related to sputtering factor.[54] Since carbon has a small sputtering yield, the etching of carbon in a polymeric species will be the slowest and therefore is a rate determining step. Etch rate is inversely proportional to the number of carbon atoms. In comparison, the number of oxygen atoms in a monomer enhance the etch rate according to the Ohnishi parameter determined from eq. (1):[54]

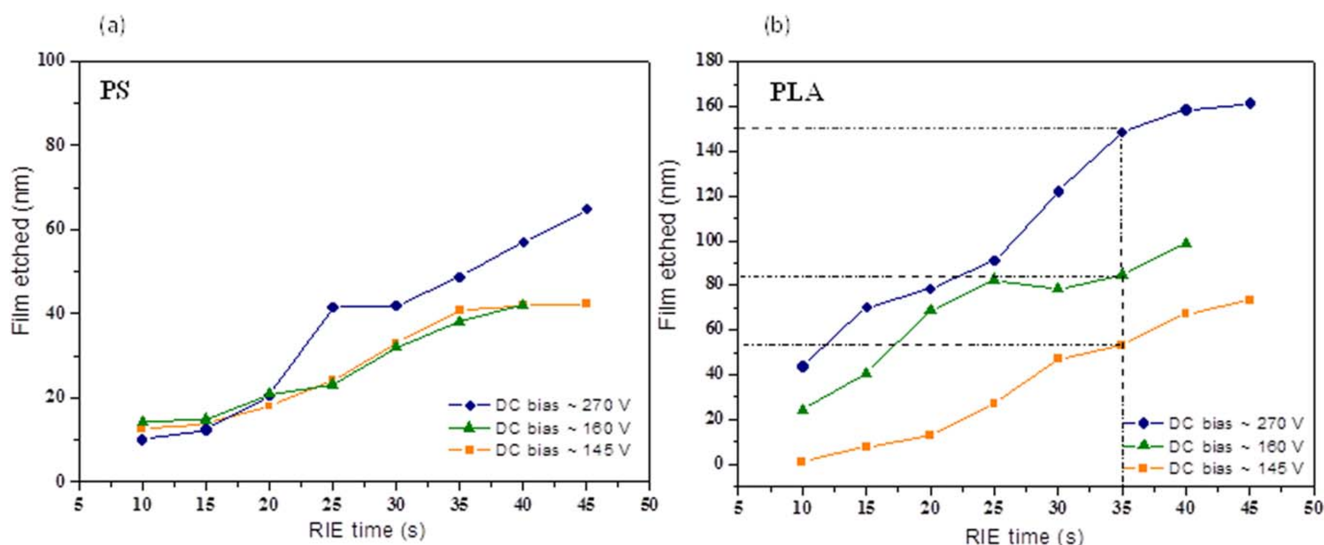

Figure 12. The effect of DC bias on etch rate. (a) PS and (b) PLA homopolymers at DC bias of 145, 260 and 270 V. The effect of DC bias is more pronounced on PLA than the PS hompolymer. [Color figure can be viewed in the online issue, which is available at wileyonlinelibrary.com.]

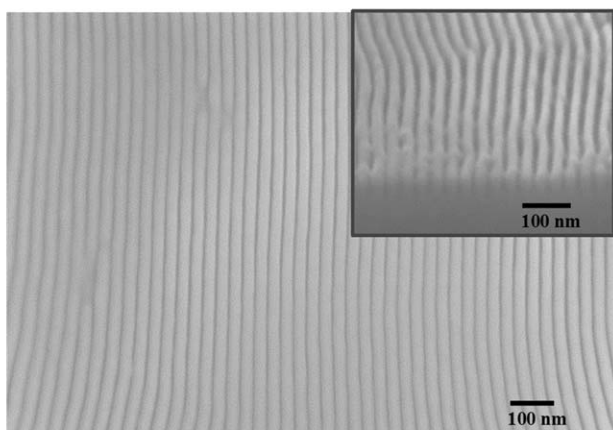

Figure 13. Top down SEM image of silicon nanowires following pattern transfer of PS soft mask template. Inset shows cross-section SEM revealing uniformity of silicon nanostructures.

$$v \propto \frac{N}{N_C - N_O} \quad (1)$$

v is the etch rate, N is the total number of atoms in a monomer unit while N_C and N_O are the number of carbon and oxygen atoms in a particular monomer unit. Since the number of carbon and oxygen atoms in PLA ($C_3H_6O_3$) are the same, the etch rate of PLA cannot be calculated theoretically. PS and PLA homopolymer etch rates have been determined in this work experimentally (see Figure 8). Although the etch rate of PS is higher at the beginning, the PLA etch rate increases at a later stage ($t > 20$ s). This higher etch rate of PLA is correlated to the presence as well as the amount of oxygen atoms in the monomer.

The RIE etch experiment was performed at different DC bias values. DC bias is a byproduct of the etch process and usually cannot be changed as a variable parameter. However, DC bias which occurs due to the imbalance of ion current and electron current is inversely proportional to process pressure $\left(DC_{bias} \propto \frac{1}{P^2}\right)$. Considering this relationship, by varying the process pressure the DC bias can be altered and tuned appropriately. The DC bias has been systematically tailored in our work (see Figure 9) by changing the process pressure.

At higher DC bias values, the PLA etch rate is higher than PS even when samples are etched for short periods. Figure 10 shows the PS and PLA rate at DC bias 270 V, where PLA is removed faster at all times during the etch. For example at $t = 35$ s, PLA is removed three times faster than PS. However, our results show the etch selectivity is not independent from DC bias (see Figure 11). Note that the etch selectivity relationship outlined in this work between PS and PLA is the ratio of PLA film removed to the etched PS layer at a given time $\left(\frac{dPLA}{dPS}\right)$. Depending on DC bias, different trends can be observed from our experimental data (see Figure 11). At lower DC bias (145 V) the etch selectivity of PS and PLA increases over time, but the increment is not dramatic and the selectivity is 1.7 at its maximum. More notably after 25 s (at DC bias 145 V), the etch selectivity remains more or less constant. However at higher DC bias i.e. 270 V, it seems there are two apparent regions. At $t < 25$ s, there is no clear trend. This is possibly due to the fact that at higher DC bias, the voltage fluctuates a lot at the beginning of RIE etch process, before it settles to the final value. This is due to higher imbalance of ions and electrons at the negative cycle of the voltage. At lower DC bias, the dispute is less predominant. For instance, in Figure 11, at DC bias 160 V and $t < 25$ s, there is a systematic increase in etch selectivity of PS and PLA with time. This trend is also seen at DC bias 145 V (i.e. at $t < 25$ s), but the etch rate is slower. More notably, in Figure 11 at $t > 25$ s denoted as region 2, the etch selectivity is higher at increased DC bias values, but it remains almost constant or with a very little change over time for all different values of DC bias. This evidently shows the effect of DC bias on etch selectivity; at shorter times, where the DC bias is fluctuating more frequently (region 1 in Figure 11) the film removal rate changes with time. At longer etch times (region 2), when the DC bias is steady, the polymer films thin at nearly a constant rate. However, in region 2, the etch selectivity at any given time is greater for higher values of DC bias. This could be due to the higher resistivity of PS to the etch conditions in comparison to PLA.

Figure 12(a,b) compares the etch rate of PS and PLA as a function of DC bias. PS etch rate is very similar at all DC bias values in particular at 145 and 160 V. For instance, at $t = 35$ s, increasing the DC bias to 270 V etches the PS film for an extra 10 nm only [Figure 12(a)]. In contrast, the etch rate of PLA is very sensitive to the DC bias. Increasing the DC bias from 145 V to 160 V and to 270 V removes PLA layers much more effectively, from 53 nm to 83 nm and 148 nm respectively, almost three times more. This explains the foremost reason for the enhanced etch selectivity between PS and PLA by DC bias; while PS etch rate remains constant, PLA is removed at a much higher rate. This contributes to higher $\left(\frac{dPLA}{dPS}\right)$ ratio. It must be

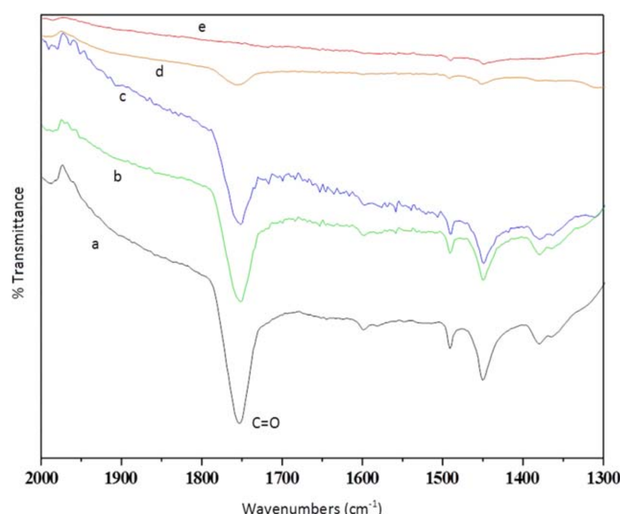

Figure 14. FT-IR spectrum showing different etch routes. (a) PS-*b*-PLA film after microphase separation and prior to etching (black line), (b) following 60 mins immersion with enzymatic approach (green), (c) 30 mins exposure with ammonium hydroxide solution (blue), (d) 20 sec etching with argon/oxygen RIE combination (orange), and (e) 45 mins immersion in 0.05*M* sodium hydroxide solution (red). [Color figure can be viewed in the online issue, which is available at wileyonlinelibrary.com.]

considered that a certain amount of PS will also be etched in the PS-*b*-PLA films during the selective etch of the PLA component. The hompolymer etch study confirms that PLA is the component that will be removed more readily, so that a soft mask PS template is formed.

Figure 13 shows silicon nanowires following pattern transfer using the PS soft mask template created from the selective dry etch process (further details are provided in the Experimental section). The top down image in Figure 13 shows uniform silicon nanowires with 16 nm feature size. Furthermore the inset reveals structures with high fidelity and a uniform etch. The etch contrast of the original polymer template is low [Figure 7(g)] from the dry etch but the resulting nanowires show high uniformity and fidelity. However the porous templates created are also ideal for metal oxide inclusion or metal evaporation techniques for fabricating a hard mask enabling higher fidelity structures to be developed following a pattern transfer process.

FT-IR Studies of Etch Routes

FT-IR studies of specific films were made and illustrative data are provided here in Figure 14 for each of the different etch routes. The characteristic PLA peak (C=O) is observed at 1758 cm^{-1}.[22,55] Other features in agreement with literature[56] include the C-H stretch at 3000 cm^{-1} from the methyl/methyne groups as well as the bands in the region 1300 to 950 cm^{-1} corresponding to the ester linkage (-CO-O-) but are not shown for the sake of brevity (see Supporting Information Figure S9). The main PLA peak (C=O) is completely absent from the film that was immersed in the NaOH solution for 45 mins and therefore the majority of PLA had been removed leaving a topographical PS pattern. A similar result was found for the PS-*b*-PLA sample that had been dry etched for 20 sec, although the reduced PLA peak suggests the existence of residual PLA material. In comparison, the 30 min NH_4OH/methanol route indicates significant PLA retention. As might be expected, Proteinase K removes PLA at a slower rate due to the associated non-aggressive nature of a biological species and is reflected in the spectrum showing the most retention of PLA of all the etch techniques. The data in the spectrum is from the film that had been treated with the enzymatic buffer solution for 1 h that shows only partial PLA removal.

CONCLUSIONS

Symmetric PS-*b*-PLA can form well-ordered microphase separated structures on silicon or SOI substrates under solvo-microwave annealing. Rather unexpectantly, even quite thick films of 200 nm form vertical lamellae despite the modified substrate interfaces favoring either PLA or PS interactions. These lamellae structures can provide robust structures as lithographic masks or porous templates if the PLA component can be readily removed. Sodium hydroxide, ammonium hydroxide, and Proteinase K can all be used to form regular topographical PS patterns. These methods are also environmentally friendly. FT-IR data confirmed that the NaOH and NH_4OH routes removed PLA to a greater degree than the Proteniase K approach. NaOH is the most rapid of the wet etches and Proteinase K the slowest but overall Proteinase K produces less damage. It appears that autocatalytic decomposition is the cause of the greater damage in the base catalyzed etches. Crystallinity is also an issue and the PLA form and its' crystallinity will need to be considered when choosing an appropriate treatment so as to optimize the removal of PLA. All wet etches show very high etch selectivity. SEM evidence reveals PLA removal greater than 50 nm for each route following treatment for a short time period. Thinner films will be studied in the future for the wet etches in order to avoid line collapse which was a possible contributing factor to the loss of pattern quality. Because of the local variations in the thick polymer films in this work, the patterns produced are inhomogeneous. The wet etch methods are not comparable to the pattern quality achieved using the dry etch (RIE) which show excellent homogeneity. Very little damage can be seen with this anisotropic etch and this is probably due to the obvious lack of any autocatalytic effects. The etch selectivity of PS and PLA homopolymer $\left(\frac{d\mathrm{PLA}}{d\mathrm{PS}}\right)$ is greatly affected by DC bias during RIE plasma process. We have demonstrated $\left(\frac{d\mathrm{PLA}}{d\mathrm{PS}}\right)$ can change from 1.7 to 3 in the range of 145 to 270 V DC bias. PS is more resistant to DC bias due to the lack of oxygen atoms in its structure. In comparison, PLA is etched faster due to the presence of oxygen. However, at lower DC bias it takes longer to break C=O bond in PLA which has a high sputtering yield. At higher DC bias when the C=O bond is broken easier PLA etch rate accelerate while PS etch rate does not show the same dramatic effect. This is the main reason for variation in etch selectivity between PS and PLA homopolymers. By calibrating the DC bias via process pressure, we have optimized the etch condition for PS-*b*-PLA. The dry etch is probably more consistent with producing lithographic processes but the wet etch methods might be more likely to be used for technologies such as membrane fabrication, low cost sensor manufacture, or polymeric bio-scaffolds requiring large area substrate production at low capital and operating costs.

ACKNOWLEDGMENTS

The authors gratefully acknowledge Science Foundation Ireland (SFI) (Grant Number 09/IN.1/602) CSET/CRANN and LAMAND NMP FP7 grant for funding this project. The authors thank Róisín Kelly and Sozaraj Rasappa for SEM assistance.

REFERENCES

1. Park, C.; Yoon, J.; Thomas, E. L. *Polymer* **2003**, *44*, 6725.
2. Black, C. T.; Ruiz, R.; Breyta, G.; Cheng, J. Y.; Colburn, M. E.; Guarini, K. W.; Kim, H. -C.; Zhang, Y. *IBM J. Res. Dev.* **2007**, *5*, 605.
3. Hamley, I. W. *Nanotechnology* **2003**, *14*, R39.
4. Ross, C. A.; Cheng, J. Y. *MRS Bull.* **2008**, *33*, 838.
5. Botiz, I.; Darling, S. B. *Mater. Today*, **2010**, *13*, 42.
6. Bates, C. M.; Maher, M. J.; Janes, D. W.; Ellison, C. J.; Willson, C. G. *Macromolecules* **2013**, *47*, 2.
7. Luo, M.; Epps, T. H. *Macromolecules* **2013**, *46*, 7567.
8. Borah, D.; Shaw, M. T.; Holmes, J. D.; Morris, M. A. *ACS Appl. Mater. Interfaces* **2013**, *5*, 2004.
9. Cushen, J. D.; Otsuka, I.; Bates, C. M.; Halila, S.; Fort, S.; Rochas, C.; Easley, J. A.; Rausch, E. L.; Thio, A.; Borsali, R.; Willson, C. G.; Ellison, C. J. *ACS Nano*, **2012**, *6*, 3424.

10. Liu, G.; Thomas, C. S.; Craig, G. S. W.; Nealey, P. F. *Adv. Funct. Mater.* **2010**, *20*, 1251.
11. Stoykovich, M. P.; Müller, M.; Kim, S. O.; Solak, H. H.; Edwards, E. W.; De Pablo, J. J.; Nealey, P. F. *Science* **2005**, *308*, 1442.
12. Stoykovich, M. P.; Kang, H.; Daoulas, K. C.; Liu, G.; Liu, C.-C.; de Pablo, J. J.; Müller, M.; Nealey, P. *F ACS Nano* **2007**, *1*, 168.
13. Farrell, R. A.; Petkov, N.; Shaw, M. T.; Djara, V.; Holmes, J. D.; Morris, M. A. *Macromolecules* **2010**, *43*, 8651.
14. Rasappa, S.; Borah, D.; Senthamaraikannan, R.; Faulkner, C. C.; Shaw, M. T.; Gleeson, P.; Holmes, J. D.; Morris, M. A. *Thin Solid Films* **2012**, *522*, 318.
15. Farrell, R. A.; Kinahan, N. T.; Hansel, S.; Stuen, K. O.; Petkov, N.; Shaw, M. T.; West, L. E.; Djara, V.; Dunne, R. J.; Varona, O. G.; Gleeson, P. G.; Jung, S. J.; Kim, H. Y.; Koleśnik, M. M.; Lutz, T.; Murray, C. P.; Holmes, J. D.; Nealey, P. F.; Duesberg, G. S.; Krstić, V.; Morris, M. A. *Nanoscale* **2012**, *4*, 3228.
16. Ting, Y. -H.; Park, S. -M.; Liu, C. -C.; Liu, X.; Himpsel, F. J.; Nealey, P. F.; Wendt, A. E. *J. Vac. Sci. Technol. B* **2008**, *26*, 1684.
17. Borah, D. T.; Shaw, M. T.; Rasappa, S.; Farrell, R. A.; O'Mahony, C.; Faulkner, C. M.; Bosea, M.; Gleeson, P.; Holmes, J. D.; Morris M. A. *J. Phys. D: Appl. Phys.* **2011**, *44*, 174012.
18. Abetz, V., Ed. Nanoporous materials from block copolymer precursors. In: Block Copolymers II (Advances in Polymer Science) (v. 2); Hillmyer, M., Ed.; Springer: Berlin Heidelberg, **2005**, *190*, pp. 137–181.
19. Ghoshal, T.; Senthamaraikannan, R.; Shaw, M. T.; Holmes, J. D.; Morris, M. A. *Nanoscale* **2012**, *4*, 7743.
20. Ghoshal, T.; Maity, T.; Senthamaraikannan, R.; Shaw, M. T.; Carolan, P.; Holmes, J. D.; Roy, Saibal.; Morris, M. A. *Sci. Rep.* **2013**, *3*, 2772.
21. Ghoshal, T.; Senthamaraikannan, R.; Shaw, M. T.; Holmes, J. D.; Morris, M. A., *Adv. Mater.* **2013**, *26*, 1207.
22. Keen, I.; Yu, A.; Cheng, H. -H.; Jack, K. S.; Nicholson, T. M.; Whittaker, A. K.; Blakey, I., *Langmuir* **2012**, *28*,15876.
23. Zalusky, A. S.; Olayo-Valles, R.; Wolf, J. H.; Hillmyer, M. A. *J. Am. Chem. Soc.* **2002**, *124*, 12761.
24. Crossland, E. J. W.; Ludwigs, S.; Hillmyer, M. A.; Steiner, U. *Soft Matter* **2007**, *3*, 94.
25. Crossland, E. J. W.; Cunha, P.; Scroggins, S.; Moratti, S.; Yurchenko, O.; Steiner, U.; Hillmyer, M. A.; Ludwigs, S. *ACS Nano* **2010**, *4*, 962.
26. Bolton, J.; Bailey, T. S.; Rzayev, J., *Nano Lett.* **2011**, *11*, 998.
27. Olayo-Valles, R.; Guo, S. W.; Lund, M. S.; Leighton, C.; Hillmyer, M. A. *Macromolecules* **2005**, *38*, 10101.
28. Baruth, A.; Rodwogin, M. D.; Shankar, A.; Erickson, M. J.; Hillmyer, M. A.; Leighton, C. *ACS Appl. Mater. Interfaces* **2011**, *3*, 3472.
29. Han, W.; Byun, M.; Zhao, L.; Rzayev, J.; Lin, Z. Q. *J. Mater. Chem.* **2011**, *21*, 14248.
30. Torres, A.; Li, S. M.; Roussos, S.; Vert, M. *J. Environ. Polym. Degrad.* **1996**, *4*, 213.
31. Cai, H.; Dave, V.; Gross, R. A.; McCarthy, S. P. *J. Polym. Sci. Part B: Polym. Phys.* **1996**, *34*, 2701.
32. Li, S.; Molina, I.; Bueno Martinez, M.; Vert, M. *J. Mater. Sci.: Mater. Med.* **2002**, *13*, 81.
33. Tsuji, H.; Kidokoro, Y.; Mochizuki, M. E. *J. Appl. Polym. Sci.* **2007**, *103*, 2064.
34. Fukushima, K.; Abbate, C.; Tabuani, D.; Gennari, M.; Camino, G. *Polym. Degrad. Stab.* **2009**, *94*, 1646.
35. Haubruge, H. G.; Jonas, A. M.; Legras, R. *Polymer* **2003**, *44*, 3229.
36. Zhang, X.; Harris, K. D.; Wu, N. L. Y.; Murphy, J. N.; Buriak, J. M., *ACS Nano* **2010**, *4*, 7021.
37. Borah, D.; Senthamaraikannan, R.; Rasappa, S.; Kosmala, B.; Holmes, J. D.; Morris, M. A. *ACS Nano* **2013**, *7*, 6583.
38. Vayer, M.; Hillmyer, M. A.; Dirany, M.; Thevenin, G.; Erre, R.; Sinturel, C. *Thin Solid Films* **2010**, *518*, 3710.
39. Borah, D.; Rasappa, S.; Senthamaraikannan, R.; Kosmala, B.; Shaw, M. T.; Holmes, J. D.; Morris, M. A. *ACS Appl. Mater. Interfaces* **2012**, *5*, 88.
40. Borah, D.; Ozmen, M.; Rasappa, S.; Shaw, M. T.; Holmes, J. D.; Morris, M. A. *Langmuir* **2013**, *29*, 2809.
41. Vayer, M.; Nguyen, T. H.; Grosso, D.; Boissiere, C.; Hillmyer, M. A.; Sinturel, C. *Macromolecules* **2011**, *44*, 8892.
42. Lo, K. -H.; Chen, M. -C.; Ho, R. -M.; Sung, H. -W. *ACS Nano* **2009**, *3*, 2660.
43. Hsueh, H. -Y.; Ho, R. -M. *Langmuir* **2012**, *28*, 8518.
44. Garlotta, D. *J. Polym. Environ.* **2001**, *9*, 63.
45. T'abi, T.; Saj'o, I. E.; Szab'o, F.; Luyt, A. S.; Kov'acs, J. G. *Express Polym. Lett.* **2010**, *4*, 659.
46. Zalusky, A. S.; Olayo-Valles, R.; Taylor, C. J.; Hillmyer, M. A. *J. Am. Chem. Soc.* **2001**, *123*, 1519.
47. de Jong, S. J.; Arias, E. R.; Rijkers, D. T. S.; van Nostrum, C. F.; Kettenes-van den Bosch, J. J.; Hennink, W. E. *Polymer* **2001**, *42*, 2795.
48. Liu, C. -C.; Nealey, P. F.; Ting, Y. -H.; Wendt, A. E. *J. Vac. Sci. Technol. B* **2007**, *25*, 1963.
49. Siparsky, G.; Voorhees, K.; Miao, F. *J. Environ. Polym. Degrad.* **1998**, *6*, 31.
50. Chen, Y.; Zhou, S.; Li, Q. *Acta Biomater.* **2011**, *7*, 1140.
51. Nugroho, P.; Mitomo, H. *Malaysian Polym. J.* **2008**, *3*, 27.
52. Zhao, L.; Byun, M.; Rzayev, J.; Lin, Z. *Macromolecules* **2009**, *42*, 9027.
53. Cheng, H. -H.; Keen, I.; Yu, A.; Chuang, Y. -M.; Blakey, I.; Jack, K. S.; Leeson, M. J.; Younkin, T. R.; Whittaker, A. K. *Proc. SPIE* **2012**, 83231O.
54. Gokan, H.; Esho, S.; Ohnishi, Y. *J. Electrochem. Soc.* **1983**, *130*, 143.
55. Amendt, M. A.; Roerdink, M.; Moench, S.; Phillip, W. A.; Cussler, E. L.; Hillmyer, M. A. *Aust. J. Chem.* **2011**, *64*, 1074.
56. Kozluca, A.; Kaitian, X.; Denkbas, B. E.; Piskin, E. *Turkish J. Chem.* **1996**, *20*, 43.